Multifunctional Profiling of Non–Small Cell Lung Cancer Using ^{18}F-FDG PET/CT and Volume Perfusion CT

Alexander W. Sauter[1], Simeon Winterstein[1], Daniel Spira[1], Juergen Hetzel[2], Maximilian Schulze[1], Mark Mueller[3], Christina Pfannenberg[1], Claus D. Claussen[1], Ernst Klotz[4], Claus Hann von Weyhern*[5], and Marius S. Horger*[1]

[1]Department of Diagnostic and Interventional Radiology, University Hospital of Tuebingen, Tuebingen, Germany; [2]Department of Oncology, Hematology, Immunology, Rheumatology and Pulmonology, University Hospital of Tuebingen, Tuebingen, Germany; [3]Department of Nuclear Medicine, University Hospital of Tuebingen, Tuebingen, Germany; [4]Computed Tomography, Siemens Healthcare, Forchheim, Germany; and [5]Institute of Pathology, University Hospital of Tuebingen, Tuebingen, Germany

The aim of this study was to investigate correlations between glucose metabolism registered by ^{18}F-FDG PET/CT and tumor perfusion quantified by volume perfusion CT and immunohistochemical markers Ki67 and microvessel density (MVD) in patients with non–small cell lung cancer (NSCLC). **Methods:** Between February 2010 and April 2011, 24 consecutive patients (21 women, 3 men; mean age ± SD, 67.6 ± 6.8 y; age range, 55.6–81.3 y) with histologically proven NSCLC (14 adenocarcinoma, 9 squamous cell lung carcinoma [SCC], and 1 mixed adenocarcinoma and SCC) underwent ^{18}F-FDG PET/CT and additional volume perfusion CT. Maximum standardized uptake value (SUV_{max}), mean SUV, and the metabolic tumor volume were used for ^{18}F-FDG uptake quantification. Blood flow (BF), blood volume (BV), flow extraction product (K^{trans}), and standardized perfusion value (SPV) were determined as CT perfusion parameters. Both perfusion parameters and ^{18}F-FDG uptake values were subsequently related to the histologic subtypes, proliferation marker Ki67, MVD according to CD34 staining, and total tumor volume. **Results:** Mean SUV, SUV_{max}, and the metabolic tumor volume (mL) were 5.8, 8.7, and 32.3, respectively, in adenocarcinoma and 8.5, 12.9, and 16.8, respectively, in SCC. Mean BF (mL/100 mL/min), mean BV (mL/100 mL), and K^{trans} (mL/100 mL/min) were 35.4, 7.3, and 27.8, respectively, in adenocarcinoma and 35.5, 10.0, and 27.8, respectively, in SCC. Moderate correlations were found between the ^{18}F-FDG PET/CT parameters and Ki67 as well as between CT perfusion parameters and MVD but not vice versa. For all tumors, the following correlations were found: between SUV_{max} and Ki67, $r = 0.762$ ($P = 0.017$); between SUV_{max} and MVD, $r = -0.237$ ($P = 0.359$); between mean BF and Ki67, $r = -0.127$ ($P = 0.626$); and between mean BF and MVD, $r = 0.467$ ($P = 0.059$). Interestingly, correlations between the BF–metabolic relationship and total tumor volume were higher in SCC ($r = 0.762$, $P = 0.017$) than in adenocarcinoma ($r = -0.0791$, $P = 0.788$). **Conclusion:** ^{18}F-FDG uptake correlates with Ki67, whereas BF, BV, and K^{trans} correlate with MVD. Therefore, ^{18}F-FDG uptake and perfusion parameters provide complementary functional information. An improved tumor profiling will be beneficial for both prognosis and therapy response evaluation in these tumors.

Key Words: ^{18}F-FDG PET/CT; CT perfusion; VPCT; NSCLC; lung cancer

J Nucl Med 2012; 53:521–529
DOI: 10.2967/jnumed.111.097865

Lung cancer is the leading cause of cancer-related death worldwide. Approximately 85%–90% of all resected lung tumors are classified as non–small-cell lung carcinoma (NSCLC). The main histologic subtypes of NSCLC are squamous cell carcinoma (SCC) and adenocarcinoma. SCC exhibits a more destructive growth pattern and lower overall survival than does adenocarcinoma (*1,2*). Currently, advanced-stage NSCLC is considered an incurable disease for which standardized chemotherapy provides only marginal improvement in overall survival at the expense of substantial morbidity and mortality (*3*). However, with the advent of novel drugs primarily targeting tumor angiogenesis (e.g., vascular endothelial growth factor receptor and endothelial growth factor receptor inhibitors), a more efficient, individualized treatment of NSCLC is intended. New immunohistochemical and molecular biomarkers have been established as prognostic factors. Microvessel density (MVD) according to CD34 staining is related to poor survival and metastatis formation (*4*), whereas the expression of Ki67 increases with the shift from preneoplasia toward invasion (*5*). Currently, imaging is advancing from purely morphologic methods toward multifunctional techniques. For many years, tumor therapy response has been assessed using cross-sectional CT according to the response evaluation criteria in solid tumors. Obrzut et al. observed that information from ^{18}F-FDG PET/CT, compared with CT alone, provided additional information aiding in the depiction of new lesions and improving therapy assessment (*6*).

The connection between in vivo imaging and in vitro biologic diagnosis is still being explored (*7*). Because of the

Received Sep. 1, 2011; revision accepted Dec. 16, 2011.
For correspondence or reprints contact: Alexander W. Sauter, Department of Diagnostic and Interventional Radiology, University Hospital of Tuebingen, Hoppe-Seyler-Strasse 3, 72076 Tuebingen, Germany.
E-mail: alexander.sauter@klinikum.uni-tuebingen.de
*Contributed equally to this work.
Published online Mar. 13, 2012.

recent developments in functional CT, we set out to address these complex pathophysiologic processes using ^{18}F-FDG PET/CT and volume perfusion CT (VPCT). Other possible techniques for measurements of tumor vascularization include ^{15}O-labeled water PET, dynamic contrast-enhanced (DCE) ultrasound, and DCE MRI. DCE ultrasound is not an option in the assessment of lung tumors because of the restriction to acoustic windows. DCE MRI has difficulties in quantifying perfusion, because the contrast medium applied shows a nonlinear correlation to its concentration. Cardiac motion artifacts and the need for breath-hold examinations are further disadvantages of DCE MRI versus VPCT.

We wanted to relate these results to the proliferation marker Ki67, angiogenetic biomarker MVD (according to CD34 staining), and histologic subtype. The question to be answered was whether both methods exhibited different correlations with Ki67 and MVD and were therefore complementary.

MATERIALS AND METHODS

Study Population

The local ethics committee approved our study, which comprised an additional VPCT measurement after standard ^{18}F-FDG PET/CT staging, and all patients provided written informed consent, including information about the radiation exposure. To be eligible, patients needed to be 18 y or older and had to have a primary lung tumor. Exclusion criteria for contrast-enhanced CT were nephropathy (defined as a serum creatinine level $>$ 150 μmol/L), known hypersensitivity to iodine-containing contrast medium, pregnancy, and untreated hyperthyroidism. Between February 2010 and April 2011, 24 patients (21 women, 3 men; mean age ± SD, 67.6 ± 6.8 y; age range, 55.6–81.3 y) were enrolled. All patients underwent ^{18}F-FDG PET/CT and CT perfusion imaging, with a mean interval of 11.5 ± 10.5 d (range, 0–35 d). Histologic subtypes included 14 adenocarcinoma, 9 SCC, and 1 mixed adenocarcinoma and SCC.

^{18}F-FDG PET/CT

Patients fasted overnight for at least 12 h. Patients with diabetes or a fasting blood glucose level above 120 mg/dL were excluded. All patients underwent PET/CT measurements on the Hi-Rez Biograph 16 (Siemens Medical Solutions), consisting of a high-resolution 3-dimensional (3D) lutetium oxyorthosilicate PET component and a 16-row multidetector CT component. A mean dose of 339.6 ± 23.2 MBq of ^{18}F-FDG was injected. The patients underwent a standard PET/CT protocol, with a whole-body scan from the skull base to the mid thigh level. PET/CT data acquisition always started with a contrast-enhanced CT scan after administration of 100–120 mL of iopromide (Ultravist 370; Bayer HealthCare Pharmaceuticals Inc.). CT included first an arterial phase scan (120 kV, 180 mAs, 0.8-mm section collimation, 0.5-s rotation time, and 5-mm reconstructed slice thickness; scan region, skull base to upper abdomen), followed by a portal venous phase scan (120 kV, 200 mAs, 1.5-mm section collimation, 0.5-s rotation time, and 5-mm reconstructed slice thickness; scan region, upper abdomen to mid thigh level). In addition, a scan of the lung was obtained in inspiration for better delineation of the lung parenchyma (120 kV, 120 mAs, 0.8-mm section collimation, 0.5-s rotation time, and 3-mm reconstructed slice thickness). PET started 58.0 ± 3.4 min after radiotracer injection, with 3 min per bed position. PET data were subsequently reconstructed into transaxial slices (matrix size, 128 × 128; voxel size, 1.78 mm; corresponding to a transaxial field of view of 45.5 × 45.5 cm) using the manufacturer-provided standard software (Fourier rebinning and a 2-dimensional ordered-subset expectation maximization algorithm with 4 iterations and 8 subsets) and a gaussian filter of 4 mm. A separate low-dose CT scan was used for attenuation correction (120 kV, 30 mAs, 1.5-mm section collimation, and 0.5-s rotation time).

Quantitative ^{18}F-FDG PET/CT Analysis

The metabolic tumor volume (mL) was defined as 3D isocontour volumes of interest (VOIs) encompassing the whole tumor with a 50% threshold value in the PET images using syngo TrueD (Siemens Healthcare). Mean at a 50% threshold and maximum standardized uptake values ($SUV_{mean\ (50\%)}$ and SUV_{max}, respectively) and the metabolic tumor volume were recorded. To also take necrosis and areas with low metabolic activity into account, a 3D freeform VOI ($SUV_{mean\ (free)}$), exactly encompassing the tumor, and a manually drawn ellipsoid VOI (mean SUV with ellipsoid VOI [$SUV_{mean\ (ellipsoid)}$]) were defined. Additionally, total tumor volume (cm^3) was measured on the CT scans using syngo Oncology (Siemens Healthcare).

CT Perfusion Imaging

The CT protocol consisted of an unenhanced low-dose chest CT scan, followed by a 6.9-cm *z*-axis coverage chest VPCT scan using an adaptive spiral scanning technique. All examinations were performed on a 128-row CT scanner (Somatom Definition AS+; Siemens Healthcare). Subsequently, the scan range was planned for coverage of the most prominent lesion. The following perfusion parameters were applied: 80 kV, 60 mAs for patients less than 70 kg and 80 mAs for patients 70 kg or more, and 128 × 0.6 mm collimation, with a total of 22 scans. The total VPCT scanning time was 40 s. During perfusion scanning, patients were asked to resume shallow breathing for the entire duration of the study. A volume of 50 mL of iopromide at a flow rate of 5 mL/s was injected in an antecubital vein through an 18-gauge needle (Vasofix; B. Braun Melsungen AG), followed by a flush of 50 mL of NaCl at 5 mL/s and a start delay of 4 s. Contrast material was administered using a dual-head pump injector (Medtron). One set of axial images with a slice thickness of 3 mm for perfusion analysis was reconstructed without overlap, using a medium smooth-tissue convolution kernel (B10f). All images were then made anonymous and transferred to an external workstation (Multi-Modality Workplace; Siemens) for further analysis.

The estimated effective dose was 3.5 mSv for men and 6.5 mSv for women (*8*).

Quantitative CT Perfusion Analysis

Data evaluation was performed with the software syngo Volume Perfusion CT Body (Siemens Healthcare). After automatic application of motion correction and noise reduction of the datasets, the software generated 3D color-coded maps of the following perfusion parameters: blood flow (BF; mL/100 mL/min), blood volume (BV; mL/100 mL), and flow extraction product (K^{trans}) (mL/100 mL/min). BF was calculated from the initial upslope section of the tissue time–attenuation curves using the maximum slope method (*9*), with $c(t)$ being the voxel enhancement and $c_A(t)$

TABLE 1
^{18}F-FDG PET/CT Parameters and Histologic Subtypes

Parameter	All	Adenocarcinoma	SCC	*P*
$SUV_{mean\ (50\%)}$	6.7 ± 3.6	5.8 ± 2.7	8.5 ± 4.3	0.156
$SUV_{mean\ (ellipsoid)}$	2.4 ± 1.2	2.3 ± 1.1	2.7 ± 1.3	0.550
$SUV_{mean\ (free)}$	5.4 ± 2.9	4.6 ± 2.2	6.8 ± 3.2	0.001
SUV_{max}	10.1 ± 5.7	8.7 ± 4.4	12.9 ± 6.6	0.176
Metabolic volume	25.2 ± 41.6	32.3 ± 51.1	16.8 ± 18.2	0.925
Total volume	67.6 ± 115.5	66.8 ± 120.3	82.0 ± 108.3	0.875

the arterial input function. BV and K^{trans} were determined using a delay-corrected modified Patlak approach (*10*):

$$\frac{c(t)}{c_A(t-\Delta t)} = \mathrm{BV} + \mathrm{K}^{\mathrm{trans}} \times \frac{\int_0^{t-\Delta t} c_A(t)dt'}{c_A(t-\Delta t)}.$$

This approach can also be derived from the 2-compartment Tofts model, with the additional assumption that the back flux of contrast material from the extra- into the intravascular space is negligible for the first 1–2 min.

Bones and other hyperdense structures were excluded with a segmentation based on Hounsfield unit values. For the arterial input function, a region of interest was placed inside the thoracic aorta. A VOI was drawn manually around the tumor in all 3 planes on the maximum-intensity-projection image sets with knowledge of the ^{18}F-FDG PET/CT data. Care was taken to exclude adjacent soft tissues (e.g., chest wall or mediastinal structures). Mean values of the whole-tumor VOI were recorded for statistical analysis. Additionally, VOIs for areas with maximal BF (mL/100 mL/min) and maximal BV (mL/100 mL) were defined.

According to Miles et al. (*11*), the standardized perfusion values (SPVs) were calculated using the following equation:

$$\mathrm{SPV} = E_{tP} \times (W/[D \times \rho_t]).$$

To measure the calibration correction factor, a lung phantom was scanned with the same CT perfusion parameters, and a factor of 41.46 Hounsfield units/mg/mL was determined.

Additionally, total tumor volume (cm^3) was measured on the CT scans using syngo Oncology (Siemens Healthcare).

Pathology Specimen and Immunohistochemistry

Tumors resected by thoracotomy or biopsies were used as pathologic specimens. Formalin-fixed, paraffin-embedded specimens were cut in 4-μm slices and affixed to glass slides. The slides were stained with hematoxylin and eosin. Eighteen of 24 specimens were then stained with immunohistochemicals to detect the expressions of Ki67 (Mib1, clone: Mib1 (8), isotope: IgG1 κ, 1:200; DakoCytomation) and CD34 (CD 34, clone: QBEnd-10, isotope: IgG1 κ, 1:50; DakoCytomation) using the specific corresponding antibodies. A pathologist who was masked to the clinical data and PET/CT and CT perfusion findings examined these histopathologic slides.

Analysis of Expression of Ki67 and MVD CD34

One thousand tumor cells were randomly chosen from the 10 high-power fields and evaluated at ×400 magnification. Ki67 was estimated by counting the percentage of Ki67-positive cell nuclei per 1,000 tumor cells in 10 visual fields of the tumor with the highest staining, mostly corresponding to those areas with the highest mitotic activity. The average number of CD34-positive capillaries and small venules was carefully counted in the 3 areas of maximal vascularization under ×400 magnification.

Statistical Methods

Descriptive statistics including mean and SD were calculated with SigmaPlot 11.0 (Systat Software, Inc.). Comparisons were performed using a Mann–Whitney *U* nonparametric (2 groups) or Kruskal–Wallis 1-way ANOVA test (>2 groups). Correlations between pairs of variables were evaluated using the Pearson product-moment coefficient. Statistical significance was assessed at a level of *P* less than 0.05.

RESULTS

The different parameters from ^{18}F-FDG PET/CT and CT perfusion were classified according to the histologic subtypes: all tumors (n = 24), adenocarcinoma (n = 14), and SCC (n = 9). The first group included 1 additional patient with mixed adenocarcinoma and SCC.

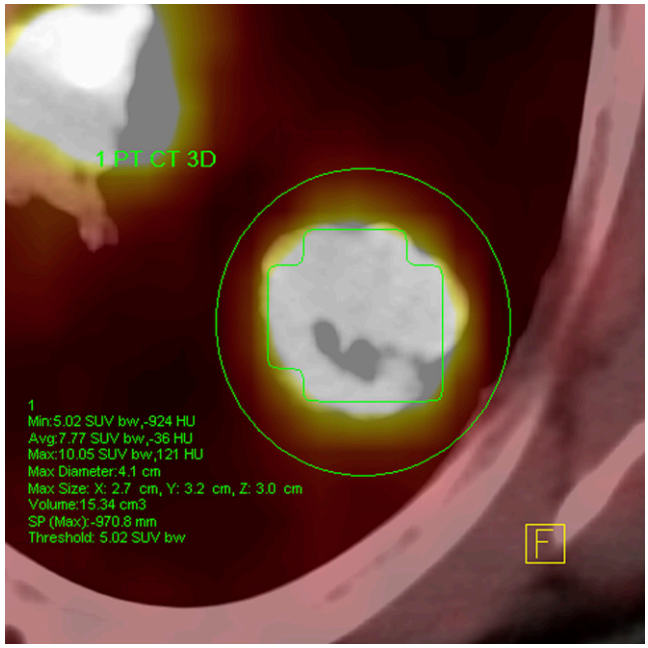

FIGURE 1. ^{18}F-FDG PET/CT image of patient with adenocarcinoma: green VOI encompasses metabolic tumor volume with 50% isocontour. Avg = average; bw = body weight; HU = Hounsfield unit; max = maximum; min = minimum.

FIGURE 2. CT scan of patient with adenocarcinoma: yellow VOI encompasses total tumor volume. RECIST = response evaluation criteria in solid tumors.

^{18}F-FDG PET/CT Parameters and Histologic Subtypes

Table 1 summarizes the mean values and the SD of $SUV_{mean\ (50\%)}$, $SUV_{mean\ (ellipsoid)}$, $SUV_{mean\ (free)}$, SUV_{max}, metabolic tumor volume (cm^3; Fig. 1), and total tumor volume (cm^3) for all tumors, adenocarcinoma, and SCC. The $SUV_{mean\ (50\%)}$ ranged from 6.7 in the all-tumors group to 5.8 in the adenocarcinoma and 8.5 in the SCC groups. Because of the enclosure of nontumoral areas within the 3D ellipsoid, the $SUV_{mean\ (ellipsoid)}$ was lower than the $SUV_{mean\ (50\%)}$—this lower value was avoided using the $SUV_{mean\ (free)}$ measurements. Interestingly, here a significant difference between the adenocarcinoma and SCC groups was present. After the SUV_{mean}, 12.9 SUV_{max} in the SCC group was higher than 8.7 SUV_{max} in the adenocarcinoma group. The metabolic tumor volume was smaller in the SCC group (16.8 cm^2) than in the adenocarcinoma group (32.2 cm^3) (Fig. 1). In contrast, total tumor volumes were 82.0 cm^3 for the SCC and 66.8 cm^3 for the adenocarcinoma groups (Fig. 2). The mean of the longest diameters was 46.5 ± 28.2 mm (range, 11.9–114.5 mm). No significant differences in these parameters and tumor grading were found between the adenocarcinoma and SCC groups (not shown).

CT Perfusion Parameters and Histologic Subtypes

Table 2 comprises the mean values and the SD of BF (mL/100 mL/min), blood volume (mL/100 mL), K^{trans} (mL/100 mL/min), and total tumor volume (mL) for all tumors, adenocarcinoma (Figs. 3–5), and SCC. Additionally, the maximal values for BF and BV were included. There were no statistical differences between the mean BF values of the all-tumors, adenocarcinoma, and SCC groups, ranging from 35.4 to 35.8 mL/100 mL/min. Mean BV (range, 7.3–10.0 mL/100 mL) and mean K^{trans} (range, 27.8–28.5 mL/100 mL/min) were close to each other in all 3 groups. The total tumor volumes of the CT perfusion group were not significantly different from the ^{18}F-FDG PET/CT group, arguing against a significant tumor growth between the 2 imaging studies. No significant differences were found between the adenocarcinoma and SCC groups for the mentioned parameters and low, intermediate, and high grading (not shown).

^{18}F-FDG PET/CT and CT Perfusion Parameters: Correlations with Ki67 and MVD

Table 3 summarizes the Pearson product moment correlation coefficients (*r*) and *P* values of the different ^{18}F-FDG PET/CT and CT perfusion parameters correlated with Ki67 and MVD. In the all-tumors group, positive correlations between $SUV_{mean\ (50\%)}$, $SUV_{mean\ (free)}$, SUV_{max}, and Ki67 are represented by Pearson product moment correlation coefficients of 0.626, 0.486, and 0.622. The CT perfusion parameters show no positive relationship with Ki67. No positive correlations were found for ^{18}F-FDG uptake values and MVD. In contrast, K^{trans} and MVD were highly correlated and also mean BF, suggesting a correlation to some degree. In the adenocarcinoma group, a high correlation between $SUV_{mean\ (50\%)}$ and Ki67 was seen. The other ^{18}F-FDG PET/CT and CT perfusion parameters reveal no positive relationship with either Ki67 or MVD. $SUV_{mean\ (50\%)}$ and SUV_{max} in the SCC group show high Pearson product moment correlation coefficients; however, the *P* values were above 0.05. Similar to the adenocarcinoma group, no correlations were found for the CT perfusion parameters and Ki67 and ^{18}F-FDG PET/CT parameters and MVD. The mean BF values were highly correlated with MVD. On

TABLE 2
CT Perfusion Parameters and Histologic Subtypes

Parameter	All	Adenocarcinoma	SCC	*P*
Mean BF	35.8 ± 13.5	35.4 ± 14.0	35.5 ± 13.0	0.986
Maximal BF	69.6 ± 28.1	75.7 ± 26.9	60.1 ± 27.5	0.176
Mean BV	8.1 ± 7.0	7.3 ± 6.3	10.0 ± 7.6	0.219
Maximal BV	20.0 ± 16.9	21.8 ± 19.5	17.2 ± 11.3	0.825
Mean K^{trans}	28.5 ± 17.5	27.8 ± 10.3	27.8 ± 25.0	0.270
Total volume	71.9 ± 114.8	65.5 ± 111.3	89.9 ± 122.2	0.777

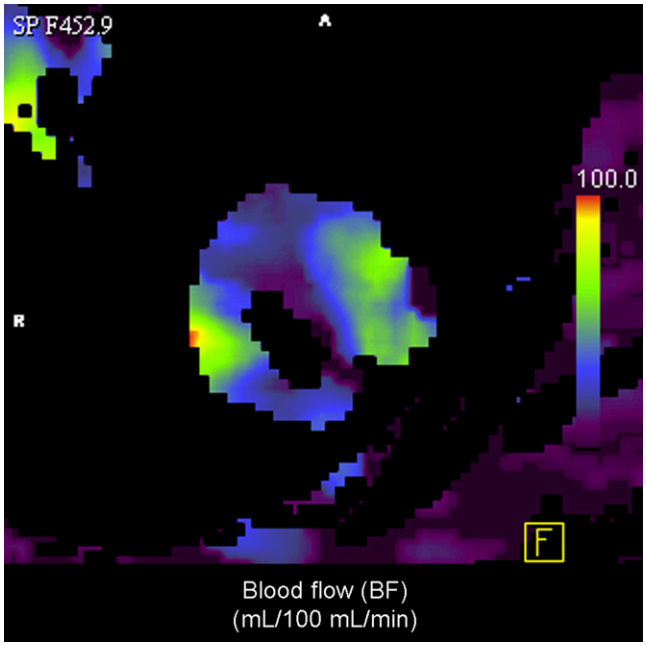

FIGURE 3. BF map of patient with adenocarcinoma.

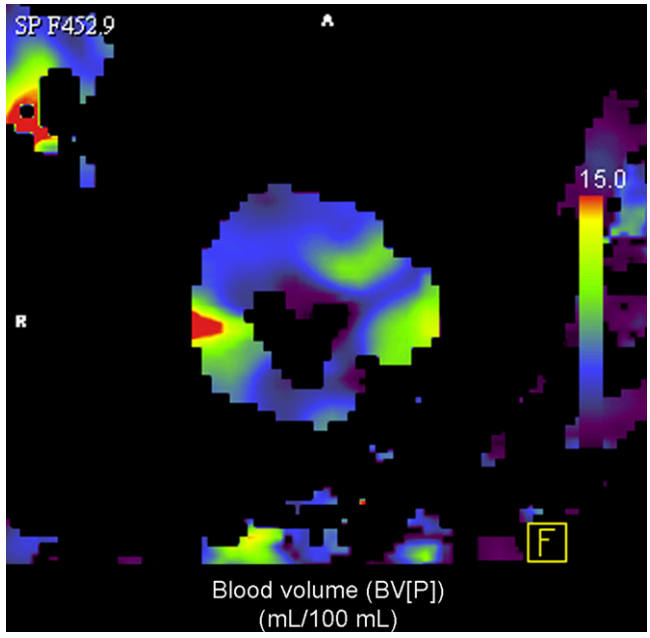

FIGURE 4. BV map of patient with adenocarcinoma.

the other hand, the maximum values for BF and BV reveal lower correlations than do the corresponding mean values.

^{18}F-FDG PET/CT and CT Perfusion Parameters: Correlations with Total Tumor Volume

Table 4 includes the Pearson product moment correlation coefficients (r) and P values of the different ^{18}F-FDG PET/CT and CT perfusion parameters correlated with total tumor volume. For this analysis, the respective means of the total tumor volumes as determined from ^{18}F-FDG PET/CT and CT perfusion datasets were used. Highly positive correlations of the tumor volume with maximal BV were found in the adenocarcinoma group and for $SUV_{mean\ (50\%)}$ and SUV_{max} in the SCC group.

BF–Metabolic Relationships Correlated with Total Tumor Volume and Histologic Subtype

Again, the means of the total tumor volumes from ^{18}F-FDG PET/CT and CT were used for this analysis. To test the reliability of the SPVs, we investigated whether there was a correlation between SPV and BF. A high correlation was represented by a product moment correlation coefficient of 0.861 and a P value of 0.000. For all tumors (Fig. 6A), no correlation between the difference in SPV and SUV_{mean} was found (SPV and $SUV_{mean\ (50\%)}$: $r = 0.314$, $P = 0.135$; SPV and $SUV_{mean\ (ellipsoid)}$: $r = -0.362$, $P = 0.082$; and SPV and $SUV_{mean\ (free)}$: $r = 0.264$, $P = 0.213$). The same holds true for the adenocarcinoma group (Fig. 6B) (SPV and $SUV_{mean\ (50\%)}$: $r = -0.0791$, $P = 0.788$; SPV and $SUV_{mean\ (ellipsoid)}$: $r = -0.318$, $P = 0.268$; and SPV and $SUV_{mean\ (free)}$: $r = -0.090$, $P = 0.759$). Interestingly, SPV–$SUV_{mean\ (50\%)}$ and SPV–$SUV_{mean\ (free)}$ reveal highly positive correlations with the total tumor volume for the SCC group (SPV and $SUV_{mean\ (50\%)}$: $r = 0.762$, $P = 0.017$; SPV and $SUV_{mean\ (ellipsoid)}$: $r = -0.381$, $P = 0.312$; and SPV and $SUV_{mean\ (free)}$: $r = 0.757$, $P = 0.018$) as shown in Figure 6C.

DISCUSSION

More sensitive and specific surrogate biomarkers are needed for tumor characterization, prognosis evaluation, and individualized therapy regimes. ^{18}F-FDG PET/CT has

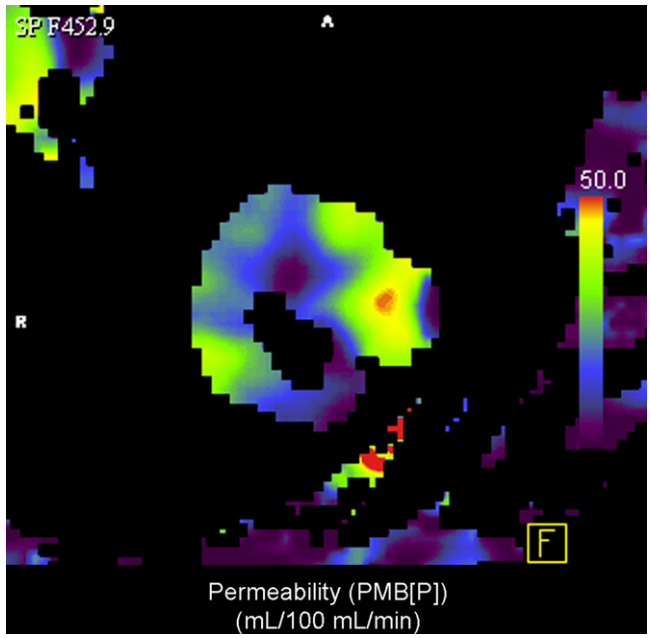

FIGURE 5. K^{trans} map of patient with adenocarcinoma.

TABLE 3
^{18}F-FDG PET/CT and CT Perfusion Parameter Correlations with Ki67 and MVD

Parameter	Ki67		MVD	
	r	*P*	*r*	*P*
All				
$SUV_{mean\ (50\%)}$	0.626	0.007	−0.248	0.337
$SUV_{mean\ (ellipsoid)}$	0.376	0.137	−0.247	0.340
$SUV_{mean\ (free)}$	0.486	0.048	−0.233	0.368
SUV_{max}	0.622	0.008	−0.237	0.359
Mean BF	−0.127	0.626	0.467	0.059
Maximal BF	−0.001	1.000	0.102	0.698
Mean BV	−0.290	0.259	0.399	0.112
Maximal BV	−0.389	0.123	0.110	0.673
Mean K^{trans}	−0.224	0.388	0.498	0.042
Adenocarcinoma				
$SUV_{mean\ (50\%)}$	0.670	0.048	−0.182	0.640
$SUV_{mean\ (ellipsoid)}$	0.147	0.707	−0.132	0.736
$SUV_{mean\ (free)}$	0.261	0.497	−0.137	0.725
SUV_{max}	0.562	0.115	−0.149	0.702
Mean BF	−0.097	0.803	0.337	0.374
Maximal BF	−0.071	0.855	−0.108	0.783
Mean BV	−0.387	0.303	0.549	0.126
Maximal BV	−0.546	0.128	0.048	0.902
Mean K^{trans}	0.013	0.974	0.499	0.171
SCC				
$SUV_{mean\ (50\%)}$	0.723	0.066	−0.204	0.661
$SUV_{mean\ (ellipsoid)}$	0.507	0.245	−0.304	0.507
$SUV_{mean\ (free)}$	0.631	0.128	−0.135	0.773
SUV_{max}	0.754	0.051	−0.187	0.689
Mean BF	−0.021	0.964	0.810	0.027
Maximal BF	0.354	0.436	0.530	0.221
Mean BV	−0.219	0.637	0.308	0.502
Maximal BV	−0.035	0.941	0.537	0.214
Mean K^{trans}	−0.382	0.397	0.123	0.793

TABLE 4
^{18}F-FDG PET/CT and CT Perfusion Parameter Correlations with Total Volume

Parameter	Total volume	
	r	*P*
All		
$SUV_{mean\ (50\%)}$	0.347	0.105
$SUV_{mean\ (ellipsoid)}$	0.413	0.045
$SUV_{mean\ (free)}$	0.378	0.069
SUV_{max}	0.381	0.073
Mean BF	−0.064	0.773
Maximal BF	0.197	0.357
Mean BV	−0.190	0.384
Maximal BV	0.372	0.074
Mean K^{trans}	−0.086	0.695
Adenocarcinoma		
$SUV_{mean\ (50\%)}$	0.045	0.880
$SUV_{mean\ (ellipsoid)}$	0.401	0.155
$SUV_{mean\ (free)}$	0.182	0.532
SUV_{max}	0.091	0.756
Mean BF	−0.072	0.808
Maximal BF	0.083	0.779
Mean BV	−0.116	0.692
Maximal BV	0.579	0.030
Mean K^{trans}	−0.035	0.904
SCC		
$SUV_{mean\ (50\%)}$	0.709	0.032
$SUV_{mean\ (ellipsoid)}$	0.394	0.295
$SUV_{mean\ (free)}$	0.610	0.081
SUV_{max}	0.745	0.021
Mean BF	−0.050	0.899
Maximal BF	0.436	0.241
Mean BV	−0.340	0.370
Maximal BV	−0.201	0.604
Mean K^{trans}	−0.141	0.717

gained wide acceptance for staging and restaging patients with NSCLC. For SUV_{max}, a strong inverse correlation with survival was observed in patients with NSCLC (*12*). Besides glucose metabolism, tumor angiogenesis plays an important role in tumor growth and metastasis. With the advent of more specific therapies for NSCLC, the demand for multiparametric tumor profiling, capable of predicting tumor aggressiveness, response, and prognosis, becomes mandatory.

Today, efforts are being made to evaluate the benefit of measuring tumor perfusion with functional CT. Zhang et al. have proposed the application of CT perfusion imaging for pulmonary nodules and studied BF patterns in a single CT scan section (*13*). This technique is based on the exchange of iodinated contrast material between the intravascular space and the extravascular interstitial space and can be easily integrated in a clinical routine setting (*14*). To further increase the perfusion coverage without enlarging the physical detector width, repeated spiral scanning and continuous table movements were combined (*10*). In 2010, Tacelli et al. applied the latest 4-dimensional spiral-mode technique for lung cancer perfusion studies using a 128-row CT scanner (*15*). Hybrid and multifunctional imaging technologies, compared with stand-alone systems, are advancing because a more sophisticated disease profiling is possible (*16,17*). In 2006, Miles et al. pioneered this field, examining the relationships between tumor BF and glucose metabolism in NSCLC (*18*).

Here, we set out to prospectively quantify perfusion parameters in NSCLC (adenocarcinoma and SCC) using the novel technique of VPCT and to look for possible correlations with ^{18}F-FDG uptake and established immunohistochemical biomarkers such as Ki67 and MVD.

Our results show no significant differences in perfusion (BF, BV, and K^{trans}) between adenocarcinomas and SCCs and grading. Positive correlations between mean BF, mean K^{trans}, and MVD were found in the entire patient cohort. However, correlation between BF and MVD reached statistical significance only in SCC. Assessment of tumor volume perfusion by VPCT showed similar results in both NSCLC groups, correlating positively with MVD but not with Ki67. Unexpectedly, the correlation between maximal BF or BV and MVD were lower than the correlation between the mean values and MVD. This lower correlation might be explained by the fact that specimen-taking and histologic preparation were not guided by these maximum

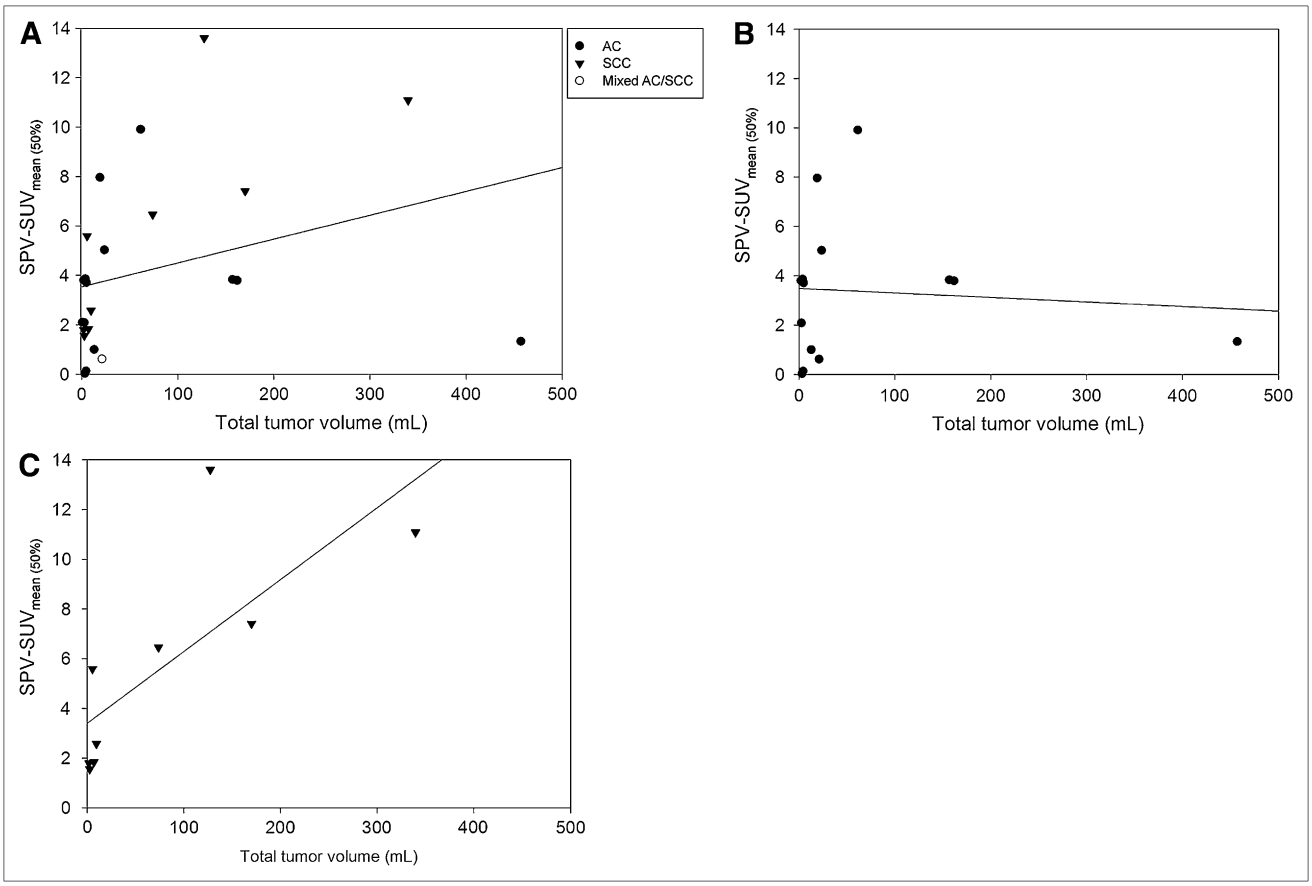

FIGURE 6. (A) BF–metabolic relationship correlated with total tumor volume in all patients (SPV and $SUV_{mean\ (50\%)}$). (B) BF–metabolic relationship correlated with total tumor volume in patients with adenocarcinoma (SPV and $SUV_{mean\ (50\%)}$). (C) BF–metabolic relationship correlated with total tumor volume in patients with SCC (SPV and $SUV_{mean\ (50\%)}$).

perfusion values. A similar attempt to find a correlation between tumor perfusion and ^{18}F-FDG uptake in NSCLC was done by Hoekstra et al. using ^{15}O-labeled water as a tracer for perfusion measurement; the authors could not ascertain any significant correlation between the 2 parameters and concluded that perfusion and glucose consumption are not coupled in NSCLC (*19*). Ng et al. demonstrated that tumor BF measurements as determined by perfusion CT and ^{15}O-labeled water PET correlate reasonably, although both methods have different physical backgrounds and instrumentations (*20*). The authors concluded that CT was better able to exclude peritumoral vessels because of its higher anatomic resolution. The inclusion of such peritumoral vessels in PET-derived regions of interest would be expected to result in higher PET estimates of BF. The main advantage of the novel VPCT technique over previous perfusion measurement techniques is the ability to calculate perfusion with short-duration scans and its independence of an on-site cyclotron. The density–time curve of tissue reaches its maximum slope before peak density (*21*). In addition to these advantages, VPCT enables whole-tumor assessment excluding sampling errors generated by previously used single-slice measurements and is empowered by robust motion correction, avoiding artifacts. However, one should take into consideration that imaging protocols and instrumentations are still under development and not yet standardized. The additional radiation exposure prohibits a careless use.

Mean standardized uptake values differed significantly only between the subgroups of SCC and adenocarcinoma when taking the entire tumor volume into account, as represented by the $SUV_{mean\ (free)}$. In our study, glucose utilization significantly correlated with tumor cell proliferation (Ki67) but not with MVD. These results are in line with other studies involved in this field of multifunctional imaging. Thus, Han et al. observed a positive correlation between SUV_{max} and Ki67 and no correlation between SUV_{max} and MVD CD34 (*7*). These findings were affirmed by other studies, for example, Guo et al. (22) and Kaira et al. (23). However, Tateishi et al. found a positive correlation ($r = 0.612$, $P < 0.001$) between SUV_{mean} and MVD (*24*). Their CT investigational protocol differed considerably from ours and was tailored for thin-slice measurements, which are less accurate. Recently, Xing et al. proposed a positive correlation between MVD and ^{18}F-FDG PET/CT (*25*). Our results do not support this proposal. They also did not yield significant differences in the distribution of Ki67 values paralleling those in ^{18}F-FDG uptake between

NSCLC subgroups, compared with Vesselle et al. (*26*). ^{18}F-FDG uptake differed among the NSCLC subtypes and correlated only with Ki67, not with MDV. Hence, the 2 imaging methods offer complementary information for tumor profiling.

Following recommendations from Miles et al., we additionally calculated the SPVs relating tissue perfusion to average whole-body perfusion and subsequently correlated results with ^{18}F-FDG uptake (*11*). We found a positive correlation between SPV and $SUV_{mean\ (50\%)}$, SPV and $SUV_{mean\ (free)}$, and total tumor volume in SCC but not in adenocarcinoma. This difference among the histologic subtypes was a new finding and might serve as a tool for an additional noninvasive tumor characterization.

Because the radiation-sensitive breast tissue was located in the range of the primary beam, the effective dose was significantly increased for female patients examined with an additional CT perfusion study (*8*). Therefore, the potential adverse effects regarding the lifetime risk for breast cancer have to be considered, especially for younger women. The decision for an additional exposure should be carefully balanced. When integrating a CT perfusion study into 1-stop-shop PET/CT examinations, reconsideration of the diagnostic CT protocols for possible dose savings are advised.

There are some limitations to this work. First, only 24 patients could be enrolled in the presented study. In addition, immunohistochemical analysis could be performed in only 18 of 24 specimens. Next, no pixel-by-pixel analysis was undertaken between SUV_{mean}, SUV_{max}, BF, BV, and K^{trans} maps. We did not correct the PET data for partial-volume effects; however, no lesion was smaller than 10 mm (*27*).

CONCLUSION

^{18}F-FDG uptake correlates with Ki67 whereas CT perfusion parameters correlate with MVD. Therefore, both noninvasive imaging modalities provide complementary information for tumor profiling. Interestingly, adenocarcinoma and SCC manifest a different BF–metabolic relationship with the total tumor volume. New hybrid imaging modalities with combined ^{18}F-FDG PET/CT and perfusion CT will therefore provide more accomplished techniques for tumor profiling, classification, prognosis, and therapy monitoring.

DISCLOSURE STATEMENT

The costs of publication of this article were defrayed in part by the payment of page charges. Therefore, and solely to indicate this fact, this article is hereby marked "advertisement" in accordance with 18 USC section 1734.

ACKNOWLEDGMENTS

We thank our technicians Nicole Sachse, Astrid Schreiber, and Henriette Heners for their excellent assistance. Siemens Healthcare supported the study. No other potential conflict of interest relevant to this article was reported.

REFERENCES

1. Maeda R, Yoshida J, Ishii G, Hishida T, Nishimura M, Nagai K. Prognostic impact of histology on early-stage non-small cell lung cancer. *Chest.* 2011;140:135–145.
2. Sardari Nia P, Van Marck E, Weyler J, Van Schil P. Prognostic value of a biologic classification of non-small-cell lung cancer into the growth patterns along with other clinical, pathological and immunohistochemical factors. *Eur J Cardiothorac Surg.* 2010;38:628–636.
3. Cataldo VD, Gibbons DL, Perez-Soler R, Quintas-Cardama A. Treatment of non-small-cell lung cancer with erlotinib or gefitinib. *N Engl J Med.* 2011;364:947–955.
4. Mineo TC, Ambrogi V, Baldi A, et al. Prognostic impact of VEGF, CD31, CD34, and CD105 expression and tumour vessel invasion after radical surgery for IB-IIA non-small cell lung cancer. *J Clin Pathol.* 2004;57:591–597.
5. Cavarga I, Kocan P, Boor A, et al. Immunohistochemical markers of proliferation and vascularisation in preneoplastic bronchial lesions and invasive non-small cell lung cancer. *Neoplasma.* 2009;56:414–421.
6. Obrzut S, Bykowski J, Badran K, Hayeri MR, Hoh CK. Utility of fluorodeoxyglucose-positron emission tomography in the identification of new lesions in lung cancer patients for the assessment of therapy response. *Nucl Med Commun.* 2010;31:1008–1015.
7. Han B, Lin S, Yu LJ, Wang RZ, Wang YY. Correlation of ^{18}F-FDG PET activity with expressions of survivin, Ki67, and CD34 in non-small-cell lung cancer. *Nucl Med Commun.* 2009;30:831–837.
8. Ketelsen D, Horger M, Buchgeister M, et al. Estimation of radiation exposure of 128-slice 4D-perfusion CT for the assessment of tumor vascularity. *Korean J Radiol.* 2010;11:547–552.
9. Miles KA. Measurement of tissue perfusion by dynamic computed tomography. *Br J Radiol.* 1991;64:409–412.
10. Haberland U, Klotz E, Abolmaali N. Performance assessment of dynamic spiral scan modes with variable pitch for quantitative perfusion computed tomography. *Invest Radiol.* 2010;45:378–386.
11. Miles KA, Griffiths MR, Fuentes MA. Standardized perfusion value: universal CT contrast enhancement scale that correlates with FDG PET in lung nodules. *Radiology.* 2001;220:548–553.
12. Okereke IC, Gangadharan SP, Kent MS, Nicotera SP, Shen C, DeCamp MM. Standard uptake value predicts survival in non-small cell lung cancer. *Ann Thorac Surg.* 2009;88:911–915, discussion 915–916.
13. Zhang M, Kono M. Solitary pulmonary nodules: evaluation of blood flow patterns with dynamic CT. *Radiology.* 1997;205:471–478.
14. Miles KA, Charnsangavej C, Lee FT, Fishman EK, Horton K, Lee TY. Application of CT in the investigation of angiogenesis in oncology. *Acad Radiol.* 2000;7:840–850.
15. Tacelli N, Remy-Jardin M, Copin MC, et al. Assessment of non-small cell lung cancer perfusion: pathologic-CT correlation in 15 patients. *Radiology.* 2010;257:863–871.
16. Beer AJ, Schwaiger M. PET of alphavbeta3-integrin and alphavbeta5-integrin expression with ^{18}F-fluciclatide for assessment of response to targeted therapy: ready for prime time? *J Nucl Med.* 2011;52:335–337.
17. de Langen AJ, van den Boogaart V, Lubberink M, et al. Monitoring response to antiangiogenic therapy in non-small cell lung cancer using imaging markers derived from PET and dynamic contrast-enhanced MRI. *J Nucl Med.* 2011;52:48–55.
18. Miles KA, Griffiths MR, Keith CJ. Blood flow-metabolic relationships are dependent on tumour size in non-small cell lung cancer: a study using quantitative contrast-enhanced computer tomography and positron emission tomography. *Eur J Nucl Med Mol Imaging.* 2006;33:22–28.
19. Hoekstra CJ, Stroobants SG, Hoekstra OS, Smit EF, Vansteenkiste JF, Lammertsma AA. Measurement of perfusion in stage IIIA-N2 non-small cell lung cancer using $H_2{}^{15}O$ and positron emission tomography. *Clin Cancer Res.* 2002;8:2109–2115.
20. Ng CS, Kodama Y, Mullani NA, et al. Tumor blood flow measured by perfusion computed tomography and ^{15}O-labeled water positron emission tomography: a comparison study. *J Comput Assist Tomogr.* 2009;33:460–465.
21. Petralia G, Preda L, Raimondi S, et al. Intra- and interobserver agreement and impact of arterial input selection in perfusion CT measurements performed in squamous cell carcinoma of the upper aerodigestive tract. *AJNR.* 2009;30:1107–1115.

22. Guo J, Higashi K, Ueda Y, et al. Microvessel density: correlation with ^{18}F-FDG uptake and prognostic impact in lung adenocarcinomas. *J Nucl Med.* 2006;47: 419–425.
23. Kaira K, Okumura T, Ohde Y, et al. Correlation between ^{18}F-FDG uptake on PET and molecular biology in metastatic pulmonary tumors. *J Nucl Med.* 2011;52: 705–711.
24. Tateishi U, Nishihara H, Tsukamoto E, Morikawa T, Tamaki N, Miyasaka K. Lung tumors evaluated with FDG-PET and dynamic CT: the relationship between vascular density and glucose metabolism. *J Comput Assist Tomogr.* 2002;26:185–190.
25. Xing N, Cai Z-l, Zhao S-h, Yang L, Xu B-x, Wang F-l. The use of CT perfusion to determine microvessel density in lung cancer: comparison with FDG-PET and pathology. *Chin J Cancer Res.* 2011;23:118–122.
26. Vesselle H, Salskov A, Turcotte E, et al. Relationship between non-small cell lung cancer FDG uptake at PET, tumor histology, and Ki-67 proliferation index. *J Thorac Oncol.* 2008;3:971–978.
27. Teo BK, Seo Y, Bacharach SL, et al. Partial-volume correction in PET: validation of an iterative postreconstruction method with phantom and patient data. *J Nucl Med.* 2007;48:802–810.